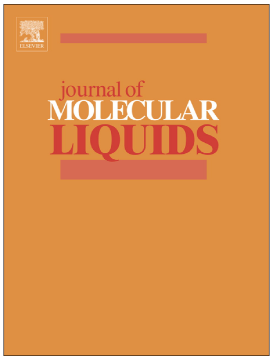

Synergistic effect of microwave rapid heating and weak mineralizer on silica-stabilized tetragonal zirconia nanoparticles for enhanced photoactivity of Bisphenol A

N.S. Hassan, A.A. Jalil, S. Triwahyono, N.F. Khusnun, S.M. Izan, K. Kidam, A. Johari

PII: S0167-7322(17)36050-6
DOI: doi:10.1016/j.molliq.2018.04.068
Reference: MOLLIQ 8971

To appear in: *Journal of Molecular Liquids*

Received date: 19 December 2017
Revised date: 22 March 2018
Accepted date: 11 April 2018

Please cite this article as: N.S. Hassan, A.A. Jalil, S. Triwahyono, N.F. Khusnun, S.M. Izan, K. Kidam, A. Johari , Synergistic effect of microwave rapid heating and weak mineralizer on silica-stabilized tetragonal zirconia nanoparticles for enhanced photoactivity of Bisphenol A. The address for the corresponding author was captured as affiliation for all authors. Please check if appropriate. Molliq(2017), doi:10.1016/j.molliq.2018.04.068

Synergistic effect of microwave rapid heating and weak mineralizer on silica-stabilized tetragonal zirconia nanoparticles for enhanced photoactivity of Bisphenol A

N.S. Hassan[a], A.A. Jalil[a,b*], S. Triwahyono[c], N.F. Khusnun[a], S.M. Izan[c], K. Kidam[a] and A. Johari[a,b]

[a]*Department of Chemical Engineering, Faculty of Chemical and Energy Engineering, Universiti Teknologi Malaysia, 81310 UTM Johor Bahru, Johor, Malaysia*

[b]*Centre of Hydrogen Energy, Institute of Future Energy, 81310 UTM Johor Bahru, Johor, Malaysia*

[c]*Department of Chemistry, Faculty of Science,Universiti Teknologi Malaysia, 81310 UTM Johor Bahru, Johor, Malaysia*

**To whom correspondence should be addressed,*

Aishah Abdul Jalil (Ph.D.)

Tel: 60-7-5535581   Fax: 60-7-5536165

Email: aishahaj@utm.my

Abstract

Silica-doped tetragonal mesoporous zirconia nanoparticles (SZ) were successfully synthesized with various concentrations of ammonia solution(NH_4OH) using microwave-assisted method for photodegradation of Bisphenol A (BPA). The phase of SZ catalyst was pure mesoporous tetragonal ZrO_2 with nano in size (5-10 nm). The increasing concentration of NH_4OH solution enhanced the hydrolysis and condensation process, as confirmed by formation of additional Zr−O−Zr, Si−O−Si and Si−O−Zr bonds. The formation of oxygen vacancy (V_o) and Zr^{3+} surface defects (ZSD) also increased proportionally with the concentration of NH_4OH solution. Both properties and the Si-O-Zr bond are supposed to play important roles in stabilizing the tetragonal phase of ZrO_2. The V_o and ZSD also lowered the band-gap energy (from 4.35 eV to 3.05 eV) and act as electron acceptors. Catalytic testing showed that 8-SZ gave the highest initial rate (0.372×10^{-3} mM min^{-1}) of 10 mg L^{-1} BPA at pH 7 using 0.5 g L^{-1} catalyst within 4 h while under similar conditions, 5-SZ, 3-SZ, 0-SZ, ZrO_2 and TiO_2 only gave 0.263×10^{-3}, 0.211×10^{-3}, 0.145×10^{-3}, 0.026×10^{-3} and 0.305×10^{-3} mM min^{-1}, respectively. These results demonstrate that higher numbers of Si−O−Zr, V_o, and ZSD seemed to be the main factors in the high photoactivity of SZ prepared in 8M NH_4OH solution (8-SZ). A kinetic study demonstrated that the photodegradation followed the pseudo-first-order Langmuir-Hinshelwood model. The mechanism study using scavenging agents proved that photogenerated hole was the main active species, thus led more hydroxyl radicals formed to degrade the BPA. The 8-SZ also exhibited a great potential on degradation of various phenols and dyes in wastewater.

Key Words **:** Silica-doped mesoporous zirconia nanoparticles; tetragonal phase; microwave; ammonium hydroxide; photoactivity

1.0 Introduction

Bisphenol A (BPA) is widely used to produce epoxy resins, polycarbonate plastics and other plastics products, which considered as a recalcitrant water contaminant that cannot be readily removed from the water due to complex aromatic molecular structure and low biodegradability [1,2]. Therefore, the treatment of such pollutant is of great interest in order to reduce the concentrations of that compounds [3]. Several methods have been explored such as adsorption, filtration, and chemical oxidation [4-6]. Nevertheless, these methods have weaknesses such as producing large amounts of sludge, time consuming, and generating secondary products [7].

An advanced oxidation process (AOPs) can be an alternative to conventional methods by heterogeneous semiconductor photocatalysts such as TiO_2, Fe_2O_3, ZnO, CuO, ZrO_2, CdS, and SnO_2 for the removal of such pollutants from wastewater [8]. Recently, ZrO_2 also has been recognized as a potential photocatalyst for the oxidation of chemicals, water splitting, and carbon dioxide reduction regardless of its wide band gap energy (5.0 eV) [9]. In fact, pure ZrO_2 has three temperature dependent stable phases: monoclinic, cubic, and tetragonal, which the latter has attracted more interest among researchers recently as a photocatalytic active material for photocatalytic degradation of dyes and phenolic compounds [10,11].
However, due to its formation has to conduct at high temperature (1100-2370ºC), various synthesis methods have been developed such as chemical precipitation, hydrothermal, and microemulsion in order to stabilize its phase at room temperature by either reducing the particles size to few nanometers or by doping which introduces defects in the lattice [12]. In addition, adjusting the reaction conditions such as precursor, pH of solution during hydrolysis, surfactant, mineralizers, processing conditions and calcination temperature also could control

the crystal growth [13]. However, those methods facing several shortcomings such as long reaction time, uneven temperature distribution, and/or, strong reduction conditions.

Over the last decade, microwave (MW)-assisted methods become an effective way to fabricate nanomaterials such as TiO_2, ZnO and Mn_2O_3 [14,15]. The uniformity and rapid heating can produce small particles with narrow size distribution and high purity than the conventional method [16,17]. Recently, we also reported a facile MW method for the synthesis of mesoporous titania and mesoporous silica nanoparticles, and its use in photocatalysis and drug delivery system, respectively [7,18]. Besides, MW also shorten the synthesis time and enhanced the crystal growth that leads to a large pore volume, pore width and surface area. Due to these advantages, an extension of this study is worth continuing. Furthermore, the studies relating the synergistic influences of MW-heating and weak mineralizer on phase stabilization of ZrO_2 nanocrystals have not been reported. In this perspective, the present work aimed to investigate the effect of concentrations of NH_4OH aqueous solution on the structure of silica-doped tetragonal mesoporous zirconia nanoparticles (SZ) that prepared via MW irradiation. The physicochemical properties of the SZ catalysts were detail characterized using XRD, TEM, surface area analysis, FTIR and ESR. The proposed structure, performance, kinetic analysis, proposed reaction mechanism, regeneration of the catalysts toward degradation of bisphenol A (BPA) as well as application on other organic pollutants are also discussed in order to confirm their responsibility in the photocatalytic reactions. The remarkable properties generated during the MW irradiation are believed could diversify its use not only in the photocatalytic reaction but also for other applications.

2.0 Experimental

2.1 *Materials*

Bisphenol A (BPA, >98% purity) was used without further purification. Hydrochloric acid (HCl), cetyltrimethylammonium bromide (CTAB), sodium hydroxide (NaOH), and 2-propanol (Pr-OH), were obtained from Merck Sdn. Bhd., Malaysia. (3-aminopropyl)triethoxysilane (APTES), ammonium hydroxide solution (NH_4OH) and Zirconium (IV) propoxide (ZrP) were obtained from QRec, Malaysia and Sigma Aldrich, respectively. 0.1 M HCl and NaOH solution were used for adjustment of pH solution.

2.2 *Preparation of catalyst*

Silica doped tetragonal mesoporous ZrO_2 was synthesized as follows; CTAB surfactant (4.68 g) was added into the mixture of propanol (120 mL), distilled water (720 mL), and 8 M NH_4OH solution (29 mL). The solution was stirred for 30 min at 323 K followed by addition of ZrP (5.7 mL) and APTES (1.053 mL) and continued for 2 h in water bath. Then, the solution was placed in the domestic microwave oven (Samsung ME711K) for heating, which was intermittently for 2 h to form a sol-gel of the SZ. The obtained sample was collected, dried and calcined at 1123 K for 3 h to give a white powder which denoted as 8-SZ catalyst. Similar procedure was performed under various NH_4OH solution concentration: 5 M, 3 M and 0 M and denoted as 5-SZ, 3-SZ and SZ, respectively. Due to the limitation, 8 M was chosen as the highest NH_4OH solution concentration that can be prepared in this study.

2.3 *Characterization*

X-ray diffraction (XRD) was used to analyze the phases of the catalysts by D8 ADVANCE Bruker X-ray diffractometer at a 2θ angle ranging from 3◦ to 90◦. Transmission electron microscope (TEM) (JEOL JEM-2100F) was used for determination of morphology and size of the catalyst. Meanwhile, Perkin Elmer Spectrum GX Fourier-transform infrared (FT-IR) Spectrometer was used to identify the functional groups of the catalysts by KBr method. The surface defect and oxygen vacancy was confirmed by ESR analysis by JEOL JESFA100 ESR spectrometer. The textural properties were determined using a Beckman Coulter SA 3100 surface area analyzer. In addition, The Kubelka-Munk (K-M) plots was used for determination of band gap and Perkin Elmer UV-Vis/DRS Spectrophotometer was used for optical absorption analysis.

2.4 Photodegradation of BPA

The experiments regarding degradation of BPA were conducted in batch reactor with four 400 W metal halide lamps (λ=400 nm) as a visible light source and a cooling system. Before being exposed to light irradiation,a desired concentration of BPA was stirred in the dark for 1 h to achieve adsorption-desorption equilibrium. Each set of experiment was conducted three times to ensure the accuracy. The pH = 7 and 10 mg L^{-1} were initial pH and concentration of BPA solution, respectively.

3.0 Results and Discussion

3.1 Catalyst characterization

3.1.1 Crystallinity, phase and structural studies

Fig. 1A shows the wide-angle XRD patterns of silica and silica-doped tetragonal zirconia nanoparticles (SZ) synthesized under various concentrations of NH_4OH solution. A broad diffraction peak centered at 2Θ= 23° was observed for SiO_2, indicating its amorphous phase (JCPDS No. 29-0085) (Fig. 1A/a) [18]. The absence of this peak in SZ catalysts may be due to its presence are too diminutive to be detected by XRD as similar phenomenon was reported when lower metal content was loaded onto ZrO_2 [19, 20]. All the SZ shown in Fig. 1A could be indexed as tetragonal phase as according to the JCPDS card No. 79-1771, the XRD diffractogram for the tetragonal phase of ZrO_2 was at peaks 29.9° (101), 34.8° (110), 50.1°(112), 59.0°(200), 60.0° (211), and 63.2°(202) (Fig. 1A/b-e) [15, 21]. The additional peaks at 59.0° and 63.2° for 5-SZ and 8-SZ demonstrated their high crystallinity compared to others, which may be evidence that the higher concentration of base improved crystal growth.

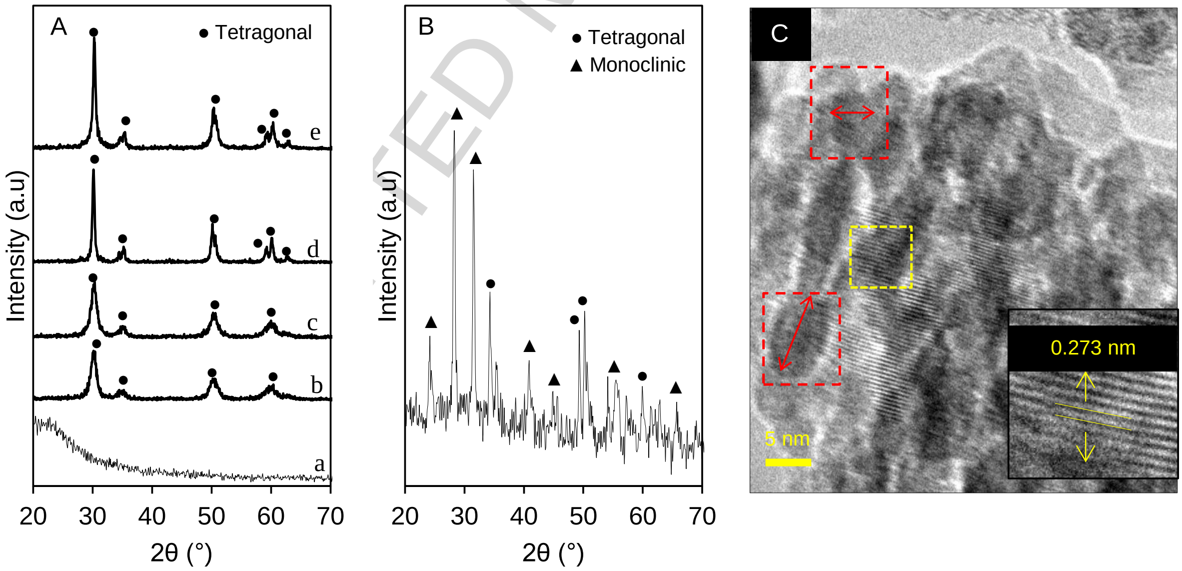

Fig. 1 XRD patterns of (A) a) SiO_2, b) SZ, c) 3-SZ, d) 5-SZ, and e) 8-SZ; (B) commercial ZrO_2 (C) TEM and HRTEM images of 8-SZ (as inset)

No reflections of monoclinic phases were observed as compared to the commercial ZrO_2 (Fig. 1B), signifying the high purity of SZ without any impurities. The peak intensities seemed increased with the increasing NH_4OH solution concentration, signifying the enhancement in the crystallinity of the SZ, which most probably due to the improvement in the structural arrangement of the ZrO_2 network [22].

Table 1 Textural properties of catalysts

Catalyst	**Surface area (m^2/g)**	**Pore volume (cm^3/g)**	**Average pore size (nm)**	**Crystallite size (nm)[a]**	**Band gap (eV)[b]**
commercial ZrO_2	7.1	0.0332	5.1	19.8	4.35
SZ	136.6	0.2653	5.1	6.3	3.75
3-SZ	130.6	0.2572	5.1	6.5	3.45
5-SZ	110.6	0.2405	6.1	8.9	3.25
8-SZ	100.7	0.1845	4.3	10.2	3.05

[a] Crystallite size calculated using Debye–Scherrer equation at $2\theta = 29.9^\circ$

[b] Band gap calculated using Kubelka–Munk (K–M) plots

The crystallite size of the SZ was calculated based on the (101) diffraction peak using the Debye-Scherer equation as follows,

$$\tau = \frac{k\lambda}{\beta \cos\theta} \tag{1}$$

where τ is particles size, k is shape factor (k = 0.9), β is the line width at half maximum height (radian), λ is the wavelength of X-ray radiation (0.15418 nm), and θ is the angular position of the peak maximum (radian). The average size of SZ crystallites ranged from 6-10 nm (Table 1). Size increased with increasing concentrations of NH_4OH solution due to the agglomeration of small crystals [23]. The broad diffraction peaks supported that the crystallites of SZ were nano in size [24]. This result was confirmed by the TEM images shown in Fig. 1C, in which the diameter of black particles of ZrO_2 were in the range of 5-10 nm (red square). While, its interplanar spacing (yellow square) was also determined to be 0.273 nm (inset figure), which implied the *d* spacing of (101) plane of tetragonal ZrO_2 (JCPDS 42-1164) [13]. These results revealed that the pure tetragonal phase of ZrO_2 with $\leq$ 10 nm of crystallite size was simply synthesized by the MW-assisted method, which are rather difficult to be produced by other conventional methods such as sol-gel and co-precipitation that mainly resulted in mixed phases [25].

3.1.2 Textural studies

The pore size distribution and nitrogen adsorption–desorption isotherms of the commercial ZrO_2 and SZ was shown in Fig. 2. For the commercial ZrO_2, a H4 hysteresis loop with type IV isotherm with was observed, which is the dominant of pore with uniform size and shape (Fig. 2A). Meanwhile, the SZ catalysts exhibited H3 hysteresis loop with isotherm type IV (Fig. 2B-E), confirming an adsorption profile for mesostructured material [26]. The filling of intraparticle pores within the samples can be observed at P/P_o=0.3-0.4, while nitrogen condensation within interparticle voids was observed at a relative pressure of 0.5-0.99. Based on the Fig. 2B-E, the intraparticle pores of SZ remain unchanged but the interparticle pores obviously reduced by the increasing NH_4OH solution concentration. Table 1 also demonstrates that the surface area and pore volume of the catalyst decreased upon addition of NH_4OH solution. The pore size distribution was shown in Fig. 2F clearly suggests that the commercial ZrO_2 possessed a very narrow monomodal pore dimension, while the SZ synthesized using the MW-assisted method were distorted to a multi-modal pore distribution by the increasing NH_4OH solution concentration, particularly after the addition of $\geq$ 5M

NH_4OH solution, which is evidence of the pore-blockage effect. This may be due to the consecutively collapsed pore walls that reduced the pore volume as well as the surface area of

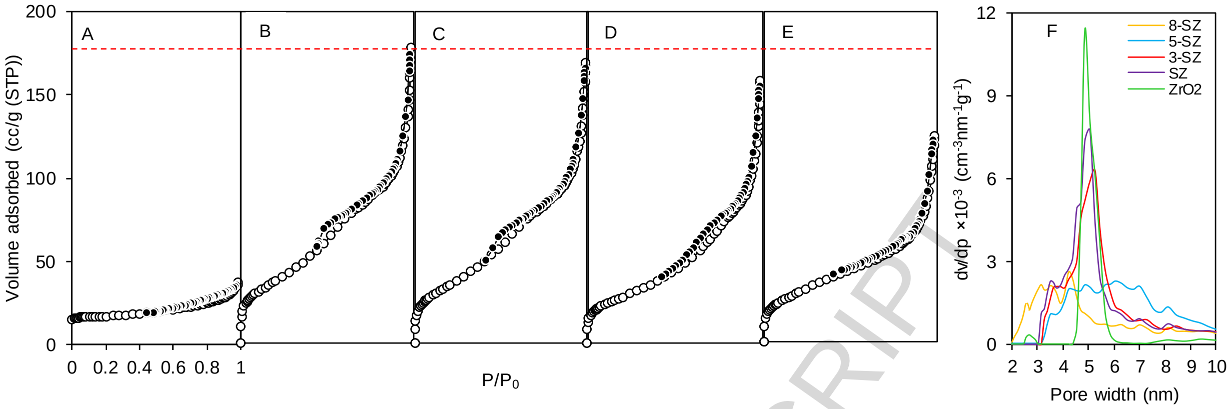

Fig. 2 N_2 adsorption-desorption isotherms plots of (A) commercial ZrO_2, (B) SZ, (C) 3-SZ, (D) 5-SZ, (E) 8-SZ, (F) Pore size distribution of catalysts

the catalysts. This result suggested the possible inclusion of silica from the APTES has interfered the arrangement of ZrO_2 matrix [27]. Similar reduction in surface area was observed when zinc was introduced into mesostructured silica nanoparticles [28].

3.1.3 Vibrational spectroscopy

A FTIR spectra of the commercial ZrO_2 and SZ in the region between 4000−400 cm^{-1} was shown in Fig 3A. The SZ catalysts displayed four main bands corresponded to −OH stretching (3456 cm^{-1}), bending vibrations of the −OH groups of the physisorbed moisture (1620 cm^{-1}), Si−O−Si asymmetric stretching (1070 cm^{-1}), and ZrO_2 skeletal (580 cm^{-1}) [29, 30]. For clarity, a Gaussian curve-fitting was plotted (Fig. S1) and the intensities of those important bands are summarized in Fig. 3B. It was seen that the Si−O−Si bonds at 1160 and 1070 cm^{-1} were increased in intensities by the increasing NH_4OH solution concentration. While, the band at 955 cm^{-1} decreased in parallel with the emergence of a new band at 950 cm^{-1}, implying the Zr ions was exchanged with the hydrogen of Si−OH groups to form new Si−O−Zr bonds. Similar interactions were observed previously when metals were supported onto mesostructured silica nanoparticles and alumina [31, 32]. The bands in range of 700−580 and 550−400 cm^{-1} also showed increasing trend which represented the stretching vibrations of Zr−O−Zr chains and tetragonal phase of ZrO_2, respectively [33, 34]. The absence of monoclinic phase was apparently seemed in all SZ catalysts as compared to commercial ZrO_2, in which the band should appear at 740 cm^{-1}. This result is in agreement with the XRD data, confirming the purity of tetragonal phase of the SZ [35]. These results suggested that the presence of Si−O−Zr bonds in the ZrO_2 network might play important role to rigorously suppress the transformation of tetragonal to monoclinic phase [36, 37]. It can be explained by the constrainment effect of the ZrO_2 particles with the surrounding amorphous silica matrix which is enough to preserve the particle growth, thus stabilized the tetragonal phase of ZrO_2 [9].

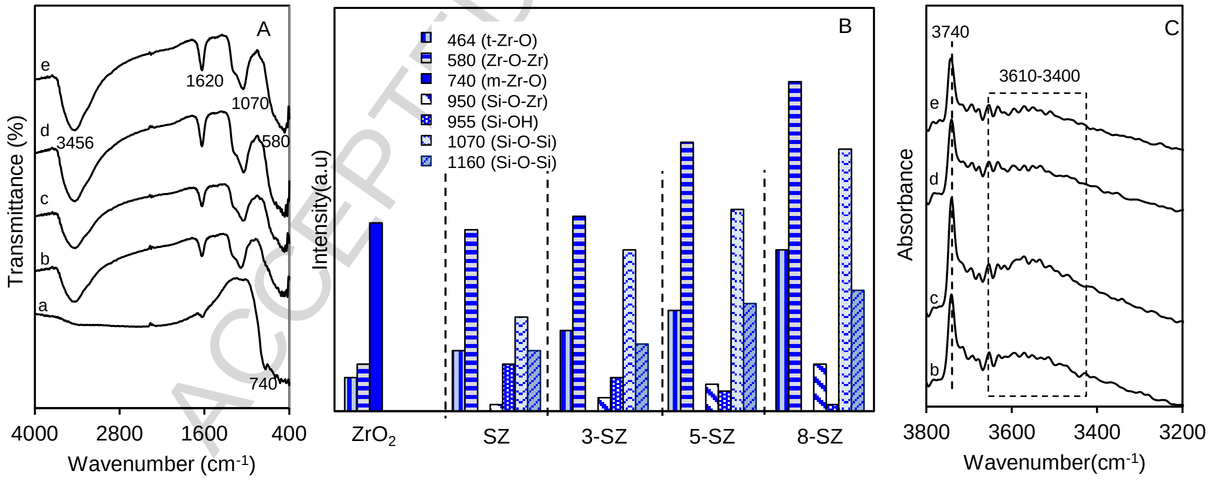

Fig. 3 (A) FTIR spectra of a) commercial ZrO_2, b) SZ, c) 3-SZ, d) 5-SZ and e) 8-SZ, (B) Intensity of Gaussian peak area in the 1300-400 cm^{-1} region, (C) IR spectra for all activated catalyst in the OH stretching region.

Next, Fig. 3C shows IR measurements for the physisorbed water by evacuating the catalysts at 623 K. The sharp band at 3740 cm^{-1}, which typically attributed to the tetragonal phase and its bibridged hydroxyl groups of the ZrO_2 framework, seemed to decrease in intensity with increasing NH_4OH solution concentration [38]. Similar result was also observed for a broad band at 3610−3450 cm^{-1}, which predictably assigned to $Zr(OH)_4$ [39]. These decreases most probably due to the fast condensation rate at higher concentration of alkaline solution that led to the formation of additional Zr−O−Zr, Si−O−Zr, and Si−O−Si bonds, as confirmed by their increasing formation at band 580, 950, 1070, and 1160 cm^{-1} in Fig. 3B.

3.1.4 Chemical oxidation state determination

In general, ESR spectroscopy is used to study the unpaired electrons as well as the occurrence of paramagnetic ions in materials. Fig. 4A shows that all SZ catalysts have similar ESR signals at g =2.011 and g=1.978, 1.951 and 1.907, which are corresponded to oxygen vacancy (V_o) and Zr^{3+} surface defect (ZSD), respectively [40, 41]. Due to similar trend, the signal of ZSD at g= 1.907 was chosen as a representative for all ZSD. It could be seen from the peaks intensities summarized in Fig. 4B that the commercial ZrO_2 possessed higher amount of ZSD but somewhat lower V_o. While, the intensities of both properties for SZ seem increased proportionally with the increasing NH_4OH solution concentration, with the 8-SZ gave the highest amount of them. It is postulated that both properties appeared due to the Zr−OH terminal bonds breaking on the SZ surface during condensation as a result of the alkaline treatment, microwave heating as well as calcination [42, 43]. In addition, uniformity of heat distribution enhanced the condensation of excess NH_4OH solution to reduce the number of OH^- ions from filling the oxygen vacancies in the lattice, thereby the higher amount of V_o could have stabilized the tetragonal phase of the ZrO_2 [13, 44]. Due to the abundant numbers of both properties, it is presumed that most of the SZ have a good prospective for the enhanced photocatalytic reaction.

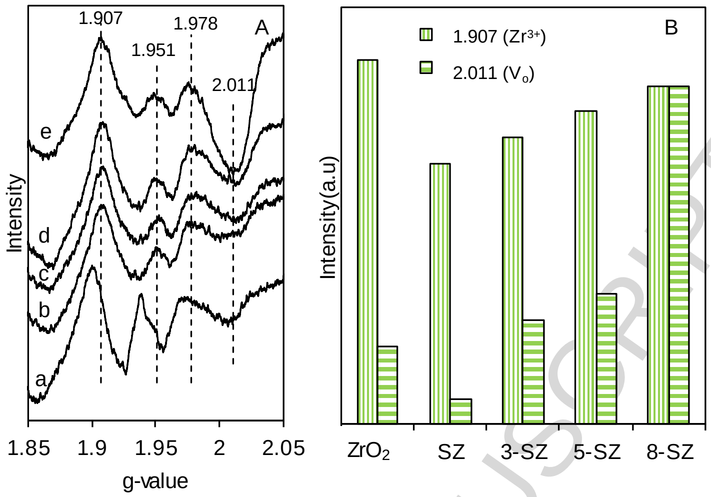

Fig. 4 (A) ESR spectra of a) commercial ZrO_2, b) SZ, c) 3-SZ, d) 5-SZ and e) 8-SZ, (B) Intensity of the related g-value

Fig S2A shows the UV-DRS spectra of all catalysts recorded at the range of 200-600 nm. Two main bands were observed at 230 and 305 nm correspond to ligand to metal charge transfer band (LMCT) from O^{2-} to an isolated Zr^{4+} ion in tetrahedral configuration [45]. Compare with commercial ZrO_2, the band for SZ was blue-shifted from 230 nm to 225 nm, signifying the decrease in its crystallite size via the addition of NH_4OH solution into the system. While, the band-gap energy of catalysts calculated by the Kubelka-Munk (K-M) equation (Fig S2B) was found to decrease by the increasing concentration of NH_4OH solution (Table 1), supporting the ESR data regarding the presence of high amount of Zr^{3+} and V_o between the valence and conduction band [46,47]. It was noticed that this result follows the quantum size effect (< 10 nm), where the band-gap energy is inversely proportional to the crystallite size of SZ catalysts [48].

3.1.5 *Proposed structure of SZ nanoparticles*

The mechanism and structure for formation of SZ are proposed regarding on the characterization results above, as in Fig 5. The CTAB created a micellar system in water-propanol media and subsequent addition of zirconium source and APTES into the prepared template formed the nanosized spheres [49]. The NH_4OH solution acted as a precipitating agent and also a basic catalyst for the hydrolysis to form $Zr(OH)_4$. Afterwards, the formation of hydroxyl and oxo-bridges between tetramer units were occurred due to polycondensation processes in the microwave via olation ($Zr{-}OH + H_2O{-}Zr \rightarrow Zr{-}OH{-}Zr + H_2O$) and oxolation ($Zr{-}OH + HO{-}Zr \rightarrow Zr{-}O{-}Zr + H_2O$) reaction [50]. The silica source underwent the process as the ZrO_2; the dramatic changes in pH mainly due to the gradual addition of NH_4OH solution and thus, accelerated both hydrolysis and condensation processes to form additional Zr−O−Zr, Si−O−Zr, and Si−O−Si bonds [22, 39]. Then, a white powder of SZ was obtained by removing the template via calcination process. On the other hand, well condensation simultaneously removed additional surface oxygen and led to the formation of V_o and ZSD. In fact, generated electrons were trapped on the Zr^{4+} sites to form Zr^{3+} [51].

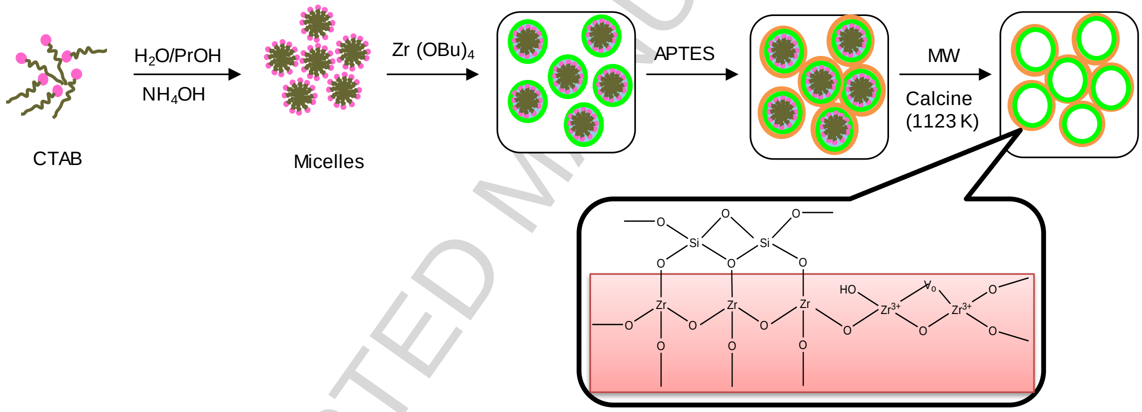

Fig. 5 Schematic diagram of formation of SZ

3.2 Photocatalytic performance and kinetic analysis

Next, the photoactivity of catalysts were examined on a degradation of BPA for 240 min and the results are illustrated in Fig. 6A. The photolysis of BPA under visible light (inset figure) shows a meagre degradation of 5% (0.006×10^{-3} mM min^{-1}), suggesting the higher stability of the pollutant. From Fig 6A, it observed that the effect of NH_4OH solution concentration demonstrated that the 8-SZ gave the highest value of 0.372×10^{-3} mM min^{-1}, followed by TiO_2, 5-SZ, 3-SZ, SZ, ZrO_2 and with 0.305×10^{-3}, 0.263×10^{-3}, 0.211×10^{-3}, 0.145×10^{-3} and 0.026×10^{-3} mM min^{-1}, respectively. The pH 7 and 0.5 g L^{-1} was the optimum condition for the highest degradation of BPA (Fig. S3A and S3B). The effectiveness of 8-SZ compared to commercial ZrO_2 most likely due to its high purity of tetragonal phase and higher numbers of V_o that led to the lowest band-gap energy [46]. The defects in crystals especially on the surface of catalysts (V_o and Zr^{3+}) play major roles in the photocatalytic

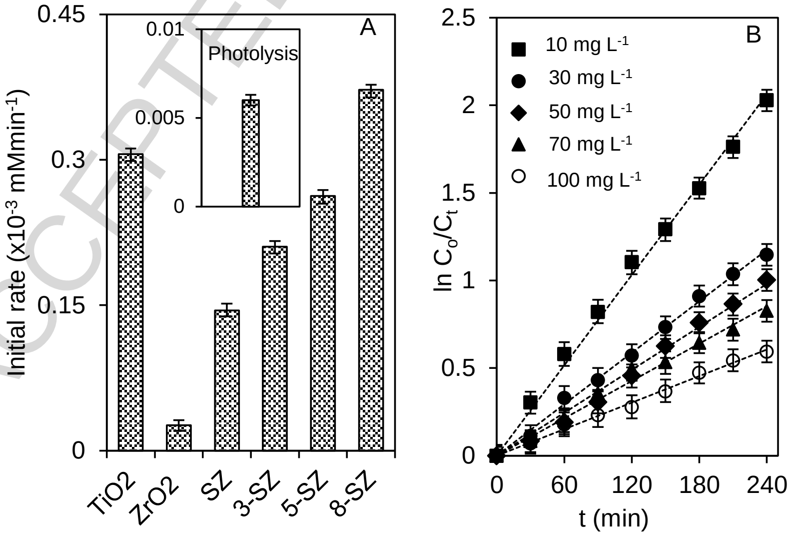

Fig. 6 (A) Catalytic performance of the catalysts under visible light towards BPA and photolysis reaction (as inset), (B) Kinetic studies of 8-SZ at different initial concentrations

reaction as active sites for the adsorption of O_2, which acts as a promoter in the oxidation of organic pollutant [52]. Similar phenomenon was reported in the degradation of 2-CP over mesoporous titania nanoparticles [7].

Table 2 The kinetics parameters of photodegradation of BPA in different initial concentration using 8-SZ

Initial concentration ($mg\ L^{-1}$)	**Reaction rate, k_{app} ($x10^{-3}\ min^{-1}$)**	**Initial reaction rate, r_o ($x10^{-2}\ mg\ L^{-1}\ min^{-1}$)**
10	8.5	8.5
30	4.8	14.4
50	4.1	20.5
70	3.6	25.2
100	2.6	26.0

The kinetics of photodegradation was studied based on the effect of initial concentration of BPA in the range of 10-100 mg L^{-1} using 8-SZ catalyst (Table 2). Fig. 6C shows the linear plot of ln (C_0/C_t) vs. irradiation time, suggesting photodegradation follows first-order which evaluated by the Langmuir–Hinshelwood model [53]. The increasing initial concentration with decrease in k_{app} values indicated that the system was favorable at low concentration. The calculated values of K_{LH} (adsorption coefficient of reactant) and k_r (reaction rate constant) for 8-SZ were 0.04968 L mg^{-1} and 0.23657 mg L^{-1} min^{-1}, respectively, in which BPA adsorption on the surface of the SZ was the controlling step of the process [7].

3.3 Proposed mechanism for photodegradation of BPA

In order to further investigation of the mechanism of BPA photodegradation, the 8-SZ catalyst was chosen and four scavenging agents were used in order to identify the key factor in the reaction: potassium peroxydisulfate (PP), ammonium oxalate (AO), isopropanol (IP) and potassium iodide (PI), which act as photogenerated electron (e^-), photogenerated hole (h^+), hydroxyl radicals (•OH) in bulk solution, and hydroxyl radicals adsorbed on the catalyst surface (•OH$_{ads}$), respectively [54]. Fig. 7A shows that the initial rate of BPA degradation decreased to 0.237× 10^{-3} mM min^{-1}, 0.269× 10^{-3} mM min^{-1}, 0.196× 10^{-3} mM min^{-1}, and 0.253 × 10^{-3} mM min^{-1} by the addition of IP, PI, AO, and PP, respectively, signifying the photogenerated hole was the main active species for degrading the BPA. Accordingly, the mechanism was proposed for degradation of BPA over SZ as in Fig. 7B. Under UV light irradiation, the holes were created at valence band (VB) caused by electrons excitation to conduction band (CB) of SZ (Eq. 2). The photogenerated holes (h^+) which have high oxidation potential, play two important roles in this degradation, in which they directly oxidized the BPA to reactive intermediate (Eq. 3), and in parallel reacted with the surface-adsorbed hydroxyl groups (OH^-) or water to yield surface-adsorbed hydroxyl radicals (•OH$_{ads}$) as shown by the decrease in degradation efficiency by PI, which then degraded the BPA (Eq. 4).

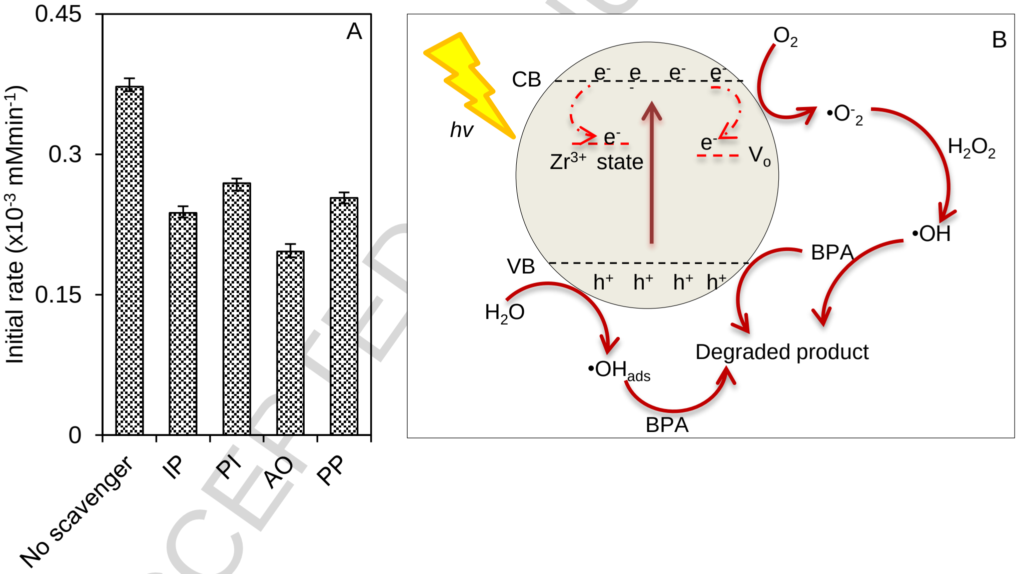

Fig. 7 (A) Photodegradation efficiencies of BPA in the presence of scavengers, (B) proposed mechanism for photodegradation of BPA over 8-SZ catalyst

$$SZ + hv \rightarrow e^- + h^+ \tag{2}$$

$$BPA + h^+ \rightarrow oxidation\ of\ BPA \tag{3}$$

$$OH^- + h^+ \rightarrow \bullet OH_{ads} \tag{4}$$

Electron-hole pair recombination was suppressed by the V_o and ZSD, which acted as electron acceptors. The electrons then reduced by the oxygen to superoxide anion radicals $\bullet O_2^-$ (Eq. 5) before reacting with H^+ in the water to produce $HOO^\bullet$ and finally generate $OH^\bullet$ for the partial or complete mineralization of BPA (Eq. 6-8) [1].

$$O_2 + e^- \rightarrow \bullet O_2^- \tag{5}$$

$$\bullet O_2^- + e^- + 2H^+ \rightarrow H_2O_2 \tag{6}$$

$$H_2O_2 + e^- \rightarrow OH^- + \bullet OH \tag{7}$$

$$\bullet OH + SZ \rightarrow \mathrm{deg}raded\ SZ \rightarrow CO_2 + H_2O \tag{8}$$

The degradation of BPA was further investigated by GC-MSD and the mechanism is proposed in Fig. 8. From the identified m/z determined by GC-MS, as well as compared with the results of previous studies, three compounds were identified as the main intermediates as presented in Fig. S4 [55]. Firstly, OH may cause cleavage between one of the benzenes and oxidize the molecules to form phenol. Then, glycolic acid and 2-butanol were formed by ring opening reaction before being finally mineralized into carbon dioxide and water.

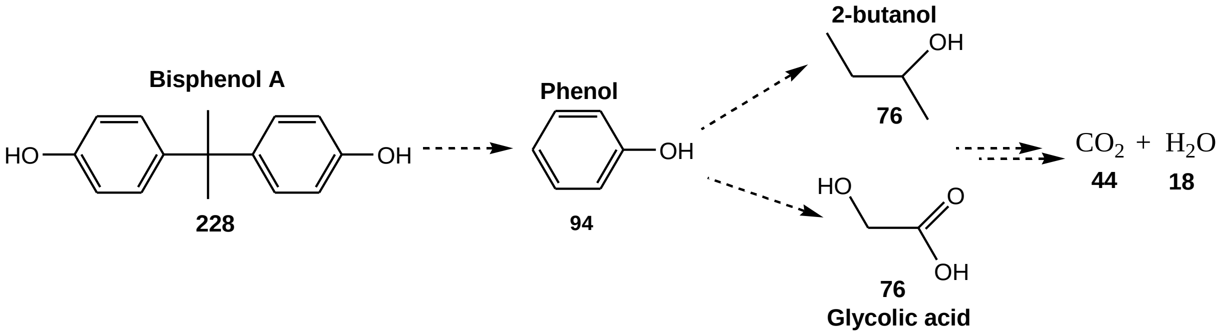

Fig. 8 Proposed mechanism of degradation BPA by GC-MSD.

3.4 Stability

The recyclability of photocatalyst is very important to their practical use. Fig. 9A shows the stability of catalyst that evaluated by repeating the experiments for five cycles using the 8-SZ catalyst. It is obviously seen that the catalyst remained active and insignificant decrease in degradation over time may be due the heat treatment which caused an aggregation of the catalyst and decreased the surface area. This result indicated that the catalyst is photochemically stable and highly reusable [56].

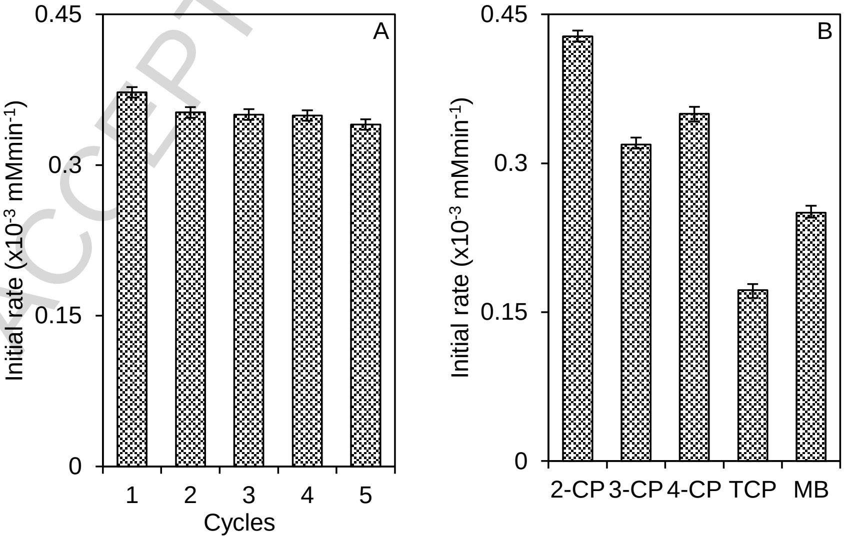

Fig. 9 (A) Stability of 8-SZ catalyst on photodegradation of BPA, (B) Photocatalytic activity of various organic pollutant.

The 8-SZ was also tested for the degradation of various organic pollutants such as 2-chlorophenol (2-CP), 3-chlorophenol (3-CP), 4-chlorophenol (4-CP), trichlorophenol (TCP), and methylene blue (MB), and the results are shown in Fig. 9B with degradation percentage of 90% (0.427×10^{-3} mM min^{-1}), 70% (0.319×10^{-3} mM min^{-1}), 75% (0.350×10^{-3} mM min^{-1}), 50%(0.170×10^{-3} mM min^{-1}), and 60% (0.252×10^{-3} mM min^{-1}), respectively. This result demonstrated that the 8-SZ has a great potential to be used for degradation of phenols and dyes wastewater.

4.0 Conclusion

As conclusion, a simple MW-assisted method was applied for preparation of silica-doped tetragonal mesoporous zirconia nanoparticles (SZ). The physicochemical properties of the catalysts were studied by XRD, TEM, N_2 adsorption-desorption, FTIR, ESR and UV-DRS analyses. Different behaviors were observed when the SZ were prepared under various concentration of NH_4OH aqueous solution. Significantly, the FTIR verified the formation of additional Zr−O−Zr, Si−O−Si, and Si−O−Zr bonds by the increasing concentration of NH_4OH solution, along with the formation of higher number of V_o and ZSD which were detected by the ESR. Those properties were found to play important roles in stabilizing the tetragonal phase of ZrO_2. The 8-SZ gave the highest value of 0.372×10^{-3} mM min^{-1}, followed by 5-SZ, 3-SZ, SZ and commercial ZrO_2 with 0.263×10^{-3}, 0.211×10^{-3}, 0.145×10^{-3} and 0.026×10^{-3} mM min^{-1}, respectively. A study of the effects of scavengers showed that the photogenerated hole was the key factor in the reaction. The Si-O-Zr, V_o and ZSD played an important role as electron acceptors to hinder the electron-hole recombination. The kinetic study showed that the degradation of BPA followed the pseudo–first-order as determined by the Langmuir–

Hinshelwood model. In addition, the regeneration test revealed that the photocatalyst remained stable even after five cycling runs. Besides stabilized the tetragonal phase of ZrO_2, the MW-assisted method also is believed could be applied for synthesis of various catalysts for various applications.

Acknowledgement

The authors are grateful for the financial support by the Fundamental Research Grant Scheme (Grant No. 14H72), awards of MyPhD Scholarship (Nurul Sahida Hassan) from the Ministry of Higher Education Malaysia and to the Hitachi Scholarship Foundation for their support.

References

[1] E. Nikfar, M. H. Dehghan, A. H. Mahvi, N. Rastkari, M. Asif, I. Tyagi, S. Agarwal, V.K. Gupta, J. Mol. Liq. 213 (2016) 332-338.

[2] P. Dhiman, M. Naushad, K.M. Batoo, A. Kumar, G. Sharma, A.A. Ghfar, A. G. Kumar, M. Singh, J. Clean. Prod. 165 (2017) 1542-1556.

[3] V. K. Gupta, S. Agarwal, H. Sadegh, G. A. M. Ali, A. K. Bharti, A. S. H. Makhlouf, J. Mol. Liq. 237 (2017) 466-472.

[4] A. Kumar, M. Naushad, A. Rana, G. Sharma, A.A. Ghfar, F.J. Stadler, M.R. Khan, Int. J. Biol. Macromol., 104 (2017) 1172-1184.

[5] M. Umar, F. Roddick, L. Fan, H.A. Aziz, Chemosphere 90 (2013) 2197–2207.

[6] J. Heo, J.R.V. Flora, N. Her, Y.-G. Park, J. Cho, A. Son, Y. Yoon, Sep. Purif. Technol. 90 (2012) 39–52.

[7] N. F. Jaafar, A. A. Jalil, S. Triwahyono, N. Shamsuddin, RSC Adv. 5 (2015) 90991-91000.

[8] J. Qin, C. Yang, M. Cao, X. Zhang, R. Saravanan, S. L, M. Ma, R. Liu, Mater. Lett. 189 (2017) 156-159.

[9] M. V. Carevic, N. D. Abazovic, T. B. Novakovic, V. B. Pavlovic, M. I. Comor, Appl Catal B. 195 (2016) 112-120.

[10] S. Zinatloo-Ajabshir, M. Salavati-Niasari, J. Mol. Liq. 216 (2016) 545–551.

[11] M. Aflaki, F. Davar, J. Mol. Liq. 221 (2016) 1071–1079.

[12] S. Shukla, S. Seal, Int. Mater. Rev. 50 (2005) 45–64.

[13] A. U. Maheswari, S. S. Kumar, M. Sivakumar, Ceram Int. 40 (2014) 6561-6568.

[14] H. Haghjoo, F. S. Sangsefidi, M. Salavati-Niasari, J. Mol. Liq 242 (2017) 779-788.

[15] R. Dwivedi, A. Maurya, A. Verma, R. Prasad, K.S. Bartwal, J. Alloys. Compd. 509 (2011) 6848-6851.

[16] Y. Kim, H. Kim, D. Jang, J. Mater. Chem. A. 2 (2014) 5791-5799.

[17] K. Hembram, G. M. Rao, J. Nanosci. Nanotechnol. 8 (2008) 4159-4162.

[18] N. H. N. Kamarudin, A. A. Jalil, S. Triwahyono, V. Artika, N. F. M. Salleh, A. H. Karim, N. F. Jaafar, M. R. Sazegarb, R. R. Mukti, B. H. Hameed, A. Johari, J. Colloid Interface Sci. 421 (2014) 6-12.

[19] K. Vignesh, A. Suganthi, B. Min, M. Kang, Appl. Surface. Sci. 324 (2015) 652-661.

[20] M. Alvarez, T. Lopez, J. A. Odriozola, M. A. Centeno, M. I. Dominguez, M. Montes, P. Quintana, D. H. Aguilar, R. D. Gonzalez, Appl. Catal., B. 73 (2007) 34-41.

[21] A. Fakhri, S. Behrouz, I. Tyagi, S. Agarwal, V. K. Gupta, J. Mol. Liq. 216 (2016) 342–346.

[22] N. W. C. Jusoh, A. A. Jalil, S. Triwahyono, A. H. Karim, N. F. Salleh, N. H. R. Annuar, N. F. Jaafar, M. L. Firmansyah, R. R. Mukti, M. W. Ali, Appl. Surf. Sci. 330 (2015) 10-19.

[23] K. D. Kim, H. T. Kim, Mater Lett. 57 (2003), 3211-3216.

[24] R. Saravanan, J. Aviles, F. Gracia, E. Mosquera, V. K. Gupta, V. K Int. J. Biol. Macromol. 109 (2018) 1239–1245.

[25] J. A. Navio, M.C. Hidalgo, G. Colon, S. G. Botta, M. I. Litter, Langmuir. 17 (2001) 202- 210.

[26] A. H. Karim, A. A. Jalil, S. Triwahyono, N. H. N. Kamarudin, A. Ripin, J. Colloid Interface Sci. 421 (2014) 93-102.

[27] K. M. Parida, S. Mallick, P.C. Sahoo, S.K. Rana, Appl. Catal., A. 381 (2010) 226-232.

[28] N. W. C. Jusoh, A. A. Jalil, S. Triwahyono, C. R. Mamat. Appl Catal A: Gen. 492 (2015) 169–176.

[29] D. M. Pickup, G. Mountjoy, G. W. Wallidge, R. J. Newport, M. E. Smith, Phys Chem Chem Phys. 1 (1999) 2527-2533.

[30] G. S. Armatas, G. Bilisb, M. Louloudib, J. Mater. Chem. 21 (2011) 2997-3005.

[31] A. F. A. Rahman, A. A. Jalil, S. Triwahyono, A. Ripin, F. F. A. Aziz, N. A. A. Fatah, N. F. Jaafar, C. N. C. Hitam, N. F. M. Salleh, N. S. Hassan. J Clean Prod. 143 (2017) 948-959.

[32] N. F. M. Salleh, A. A. Jalil, S. Triwahyono, J. Efendi, R.R. Mukti, B.H. Hameed, Appl. Surf. Sci. 349 (2015) 485-495.

[33] L. P. Borilo, L. N. Spivakova, J. Mater. Sci. 2 (2012) 119-124.

[34] T. R. Gaydhankar, R. K. Jha, M. D. Nikalje, K. J. Waghmare, Mater. Res. Bull. 55 (2014) 8-12.

[35] X. Yan, N. Lu, B. Fan, J. Bao, D. Pan, M. Wang, R. Li, Cryst. Eng. Comm, 17 (2015) 6426-6433.

[36] S. Vasanthavel, P. N. Kumar, S. Kannan, J. Am. Ceram. Soc. 97 (2014) 635-642.

[37] F. Monte, W. Larsen, J. D. Mackenzie, J. Am. Ceram. Soc. 83 (2000) 628-634.

[38] S. Kouva, K. Honkala, L. Leffertsac, J. Kanervo, Catal. Sci. Technol. 5 (2015) 3473-3490.

[39] I. A. Siddiquey, T. Furusawa, M. Sato, N. M. Bahadur, M. N. Uddin, N. Suzuki, Ceram. Int. 7 (2013) 1755-1760.

[40] T. Riemer, H. Knozinger, J. Phys. Chem. 100 (1996) 6739-6742.

[41] C. Gionco, M. C. Paganini, E. Giamello, R. Burgess, C. D. Valentin, G. Pacchioni, Chem. Mater. 25 (2013) 2243-2253.

[42] H. Eltejaei, J. Towfighi, H. R. Bozorgzadeh, M. R. Omidkhah, A. Zamaniyan, Mater. Lett. 65 (2011) 2913-2916.

[43] O. Gorban, S. Synyakina, G. Volkova, S. Gorban, T. Konstantiova, S. Lyubchik, J. Solid State Chem. 232 (2015) 249-255.

[44] K.-H. Jacob, E. Knözinger, S. Benfer, J. Mater Chem. 3 (1993) 651-657.

[45] S. K. Das, M. K. Bhunia, A. K. Sinha, A. Bhaumik, J. Phys. Chem. C. 113 (2009) 8918-8923.

[46] M. Romero-Sáez, L. Y. Jaramillo, R. Saravanan, N. Benito, E. Pabón, E. Mosquera, F. Gracia, Express Polym Lett. 11 (2017) 899–909.

[47] R.Saravanan, S. Agarwal, V. K. Gupta, M. M. Khan, F. Gracia, E. Mosquera, V. Narayanan, and A. Stephen, J. Photochem. Photobiol, A. 353 (2018) 499-506.

[48] H.-S. Lee, C.-S. Woo, B.-K. Youn, S.-Y. Kim, S.-T. Oh, Y.-E. Sung, H.-I. Lee. Top. Catal. 35 (2005) 3-4.

[49] J. Zhang, B. Song, W. Peng, Y. Feng, B. Xu, Mater. Chem. Phys. 123 (2010) 606-609.

[50] A. Adamski, P.Jakubus, Z. Sojka, Solid State Phenomen. 128 (2007) 89-96.

[51] C. Gionco, M. C. Paganini, M. Chiesa, S. Maurelli, S. Livraghi, E. Giamello, Appl. Catal, A. 504 (2015) 338-343.

[52] K. Suriye, P. Praserthdam, B. Jongsomjit, Appl. Surf. Sci. 253 (2007) 3849-3855.

[53] C. N. C. Hitam, A. A. Jalil, S. Triwahyono, A. Ahmad, N. F. Jaafar, N. Salamun, N. A. A. Fatah, L. P. Teh, N. F. Khusnun, Z. Ghazali, RSC Adv. 6 (2016) 76259–76268.

[54] N. F. Khusnun, A. A. Jalil, S. Triwahyono, N. W. C. Jusoh, A. Johari, K. Kidam. Phys Chem Chem Phys. 18 (2016) 12323-12331.

[55] Ding Y, Zhou P, Tang H, Chem Eng J. 291 (2016) 149–160.

[56] F. H. Mustapha, A. A. Jalil, M. Mohamed, S. Triwahyono, N. S. Hassan, N. F. Khusnun, C. N. C. Hitam, A. F. A. Rahman, M. L. Firmanshah, A. S. Zolkifli, J Clean Prod. 168 (2017) 1150-1162

Graphical abstract

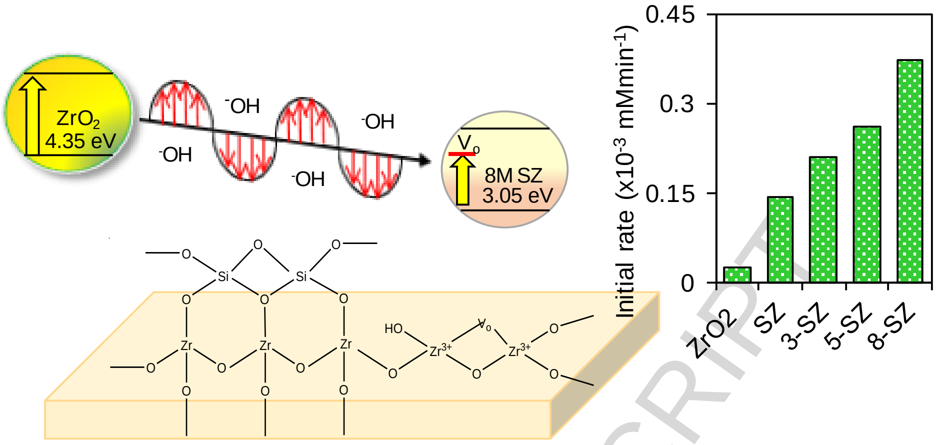

Research Highlights

- Oxygen vacancies (V_o) and silica stabilized the tetragonal structure of ZrO_2
- Microwave irradiation generated V_o and Zr^{3+} surface defects (ZSD) in ZrO_2
- Increased NH_4OH solution concentration greatly enhanced hydrolysis
- V_o and ZSD lowered the band gap of SZ from 4.35 to 3.05 eV
- 8M SZ showed the highest initial rate of degradation (0.372×10^{-3} mM min^{-1}) of bisphenol A